Physics – Uspekhi **58** (1) 61 – 70 (2015)

PHYSICS OF OUR DAYS

PACS numbers: **11.80. – m**, 13.85.Dz, 14.20.Dh

Interaction region of high energy protons

I M Dremin

DOI: 10.3367/UFNe.0185.201501d.0065

Contents

1. **Introduction** **61**
2. **Main facts and relations** **62**
3. **Geometry of the interaction region** **63**
4. **New tendencies of inelastic collisions** **67**
5. **Elastic scattering outside the diffraction cone** **68**
6. **Conclusions** **70**

References **70**

Abstract. **New proton–proton collision data from the LHC have considerably extended the energy range over which the structure of the proton–proton interaction region can be studied. In this paper, we combine the unitarity relation with experimental data on elastic scattering in the diffraction cone to show how the shape and the darkness of the inelastic interaction region of colliding protons change with increasing the proton energy. In particular, at LHC energies, small-impact-parameter collisions become fully absorptive, with some implications for inelastic processes as well. The possibility of changing from the black-core scenario at LHC energies to the fully transparent scenario at higher energies is discussed — a phenomenon that implies changing from the black disk to black toroid terminology. As the asymptotic behavior is approached, a different regime may arise. The parameter determining the opacity of central collisions also crucially affects the differential cross section of elastic scattering outside the diffraction cone, where all phenomenological models fail for the LHC energies. It is in this region where the ratio of the real to imaginary part of the elastic scattering amplitude in nonforward scattering becomes a decisive factor, as indeed it should according to the unitarity condition. Our results make it possible for the first time to estimate this ratio outside the diffraction cone by comparing with data for LHC energies, and it turns out to be drastically different from the values measured at forward scattering. Moreover, both real and imaginary parts are found to behave differently in different phenomenological models and in the approach based on the unitarity condition. This problem is still to be resolved. All the conclusions are made solely in the framework of the indubitable unitarity condition using experimental data on elastic proton scattering in the diffraction cone, without resorting to other theoretical methods, such as quantum chromodynamics or phenomenological models.**

Keywords: Protons, interaction region, elastic scattering, inelastic processes, unitarity condition

I M Dremin Lebedev Physical Institute, Russian Academy of Sciences, Leninskii prosp. 53, 119991 Moscow, Russian Federation
Tel. +7 (499) 783 37 19. Fax +7 (499) 135 78 80
E-mail: dremin@lpi.ru
National Research Nuclear University MEPhI
(Moscow Engineering Physics Institute),
Kashirskoe shosse 31, 115409 Moscow, Russian Federation

Received 23 May 2014, revised 3 June 2014
Uspekhi Fizicheskikh Nauk **185** (1) 65 – 76 (2015)
DOI: 10.3367/UFNr.0185.201501d.0065
Translated by I M Dremin; edited by A M Semikhatov

1. Introduction

In this paper, we concentrate on two problems that have become of topical interest in connection with experiments on particle interactions done at the highest available energies of the Large Hadron Collider (LHC) at CERN (Switzerland). To be more specific, our knowledge of the shape and opacity of the interaction region of two colliding protons and the behavior of their elastic scattering amplitude at various transferred momenta are discussed here. We try to present them in the way most suitable to beginners.

The general common approach to both problems, considering the irrefutable statement that the total probability of all possible processes must be equal to 1, is used in what follows. It is called the unitarity condition and is applied to information extracted from experiments on the elastic scattering of protons at small angles within the diffraction cone for the first problem and at larger angles outside the cone for the second problem. The generality of the approach guarantees the certainty of the obtained results. At the same time, it cannot of course substitute for knowledge of the dynamics of the process but helps reach some interesting conclusions about the problems to be approached. That is especially important in view of the limited applicability of QCD to a quantitative description of experimental data. In addition, some results of phenomenological models are briefly discussed. The use in the present paper of **only** these two indubitable ingredients — the unitarity condition and experimental results on elastic scattering — is decisive for providing confidence in the derived conclusions.

Why are these problems so important?

Knowledge of the elastic scattering amplitude in a wide range of energies and scattering angles would provide some guides for QCD, which has barely been applied yet to this process. Several attempts to use diagrams of the elastic scattering of hadrons containing incoherent quarks and

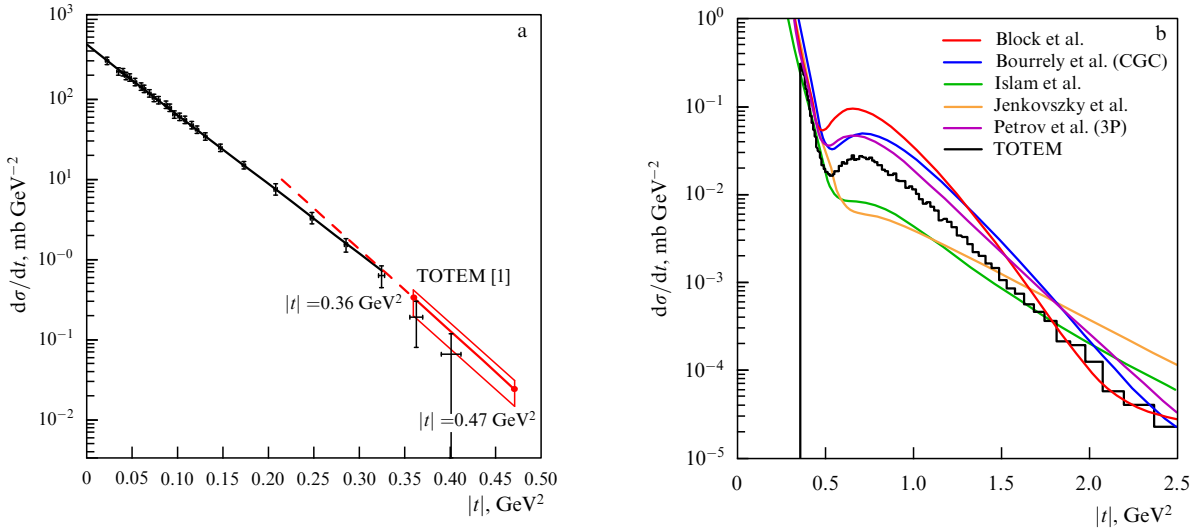

Figure 1. Differential cross section of elastic proton–proton scattering at the energy $\sqrt{s} = 7$ TeV measured by the TOTEM (TOTal Elastic and diffractive cross section Measurement) collaboration. (a) The region of the diffraction cone with the $|t|$-exponential decrease [1]. (b) The region beyond the diffraction peak [2]. The predictions of five models are demonstrated.

gluons were made only in the asymptotic freedom regime of QCD at large transverse momenta with some phenomenological arguments added. The small-angle scattering would likely require taking the coherent states of partons in the initial protons into account. The lack of this knowledge prevents further progress in this field. Any guesses from experiment about the behavior of the real and imaginary parts of the amplitude are very desirable.

The parton content of hadrons and their spatial interaction region help visualize the collision processes and compare them at different energies. The decisive role is here played by information on elastic scattering at rather small angles in the diffraction cone, from which we learn about the special regime with the black central core of the interaction region of protons with a total energy of 7 TeV in the center-of-mass system, observed at the LHC. Notably, this knowledge helps in developing some models of inelastic processes when their contribution to the unitarity relation is disentangled from elastic terms. Moreover, one can speculate on the further evolution of the spatial region with energy leading to some intriguing predictions.

Definite conclusions about the transverse momentum dependence (but, unfortunately, not about the energy dependence) of the elastic scattering amplitude at larger angles were obtained from the unitarity condition, albeit with some adjustable parameters. Fits of experimental data in this region require a noticeably enhanced role for the real part of the amplitude compared to the diffraction cone. As regards phenomenological models, their first attempts to predict the outcome of LHC experiments outside the diffraction cone failed. Their special feature is the zero of the imaginary part at the position of the dip of the differential cross section. No such zero is required by the unitarity condition. To date, there has been no consensus among these approaches about the behavior of the elastic scattering amplitude there.

2. Main facts and relations

Colliding high-energy hadrons can either scatter elastically when only two of them appear at the final stage without changing their nature or produce some new particles in inelastic processes. The kinematics of elastic scattering are very simple. They are described by two variables: the squared total energy $s = 4E^2$, where E is the energy of one of the partners in the center-of-mass system, and the four-momentum transfer squared, $-t = 2p^2(1 - \cos\theta)$, with θ denoting the scattering angle and p the momentum in the center-of-mass system. For inelastic processes, the kinematics are much more complicated. Therefore, to avoid some complications, it is quite natural to try to gain some knowledge about the dynamics of the whole process at the first stage, starting from an analysis of elastic scattering and using a general relation, the unitarity condition. This follows from the irrefutable statement that the total probability of all (elastic + inelastic) processes must be equal to 1. In this way, it relates these two channels of the reaction, albeit in a rather average, integrated form. This is the main thrust of the approach adopted in this paper.

The experimental data about elastic scattering at a given energy are not very abundant. The only information about this process comes from the measurement of the differential cross section as a function of the transferred momentum at the experimentally available values of t and of the ratio of the real and imaginary parts of the elastic scattering amplitude $f(s,t)$ $\rho(s,t) = \mathrm{Re}\, f(s,t)/\mathrm{Im}\, f(s,t)$ just in the forward direction $t = 0$ $\rho(s,0) = \rho_0$ but not at any other values of t. This ratio is obtained from studies of interference between the nuclear and Coulomb contributions to the amplitude f, which becomes practically noticeable only in the near-forward direction.

The differential cross section is related to the scattering amplitude $f(s,t)$ as

$$\frac{\mathrm{d}\sigma}{\mathrm{d}t} = \left|f(s,t)\right|^2 . \tag{1}$$

Thus, from measurements of the differential cross section at any energy of colliding particles, we acquire information only about the modulus of the amplitude at the experimentally available values of t. Typical shapes of the differential cross section at small and larger values of $|t|$ are demonstrated for the LHC energy $\sqrt{s} = 7$ TeV in Fig. 1, borrowed from [1, 2].

The most prominent feature of the plots in Fig. 1 is the fast decrease in the differential cross section with increasing the transferred momentum $|t|$. As a first approximation at present energies, it can be described at comparatively small transferred momenta in Fig. 1a by the exponential shape with the slope B such that

$$\frac{\mathrm{d}\sigma}{\mathrm{d}t} = \frac{\sigma_{\mathrm{t}}^2}{16\pi} \exp\left(-B|t|\right), \tag{2}$$

where σ_{t} denotes the total cross section. This region is called the diffraction peak. The peak becomes higher and its width shrinks with increasing energy, because both the cross section and the slope increase with energy. The slope slightly depends on t if more careful fits of experimental data are attempted, as seen in Fig. 1a. It diminishes somewhat at energies up to the ISR (Intersecting Storage Rings) energies with increasing the transferred momentum, while it starts increasing at the LHC energy 7 TeV (Fig. 1a). Moreover, some oscillations around the exponential were found in [3] at the energy $\sqrt{s} \approx 11$ GeV. A review of the early data can be found in [4]. Interesting in and of themselves, these details are not very important for our approach because only integrals of (2) are used in what follows, and such details can then be taken into account by a slight variation of B. In fact, the values of B at small $|t| < 0.3$ GeV^2 are important.

At larger values of $|t|$ outside the peak, we observe the dip and slower decrease in the plots with $|t|$ than in the diffraction cone (Fig. 1b). We note that the normalization of the amplitude is fixed by Eqns (1) and (2).

To separate the real and imaginary parts of the amplitude from the ratio ρ, one needs help from theorists. On the theoretical side, the most reliable information comes from the unitarity condition. The unitarity of the S-matrix, $SS^+ = 1$, imposes definite requirements on the behavior of the elastic scattering amplitude $f(s,t)$ and the amplitudes of inelastic processes M_i. In the s-channel, this behavior is described as [5, 6]

$$\begin{aligned}\operatorname{Im} f(p,\theta) &= I_2(p,\theta) + g(p,\theta)\\ &= \frac{s}{8\pi^{3/2}} \iint \mathrm{d}\theta_1\, \mathrm{d}\theta_2\, \sin\theta_1 \sin\theta_2\, f(p,\theta_1) f^*(p,\theta_2)\\ &\times \frac{1}{\sqrt{\left[\cos\theta - \cos\left(\theta_1+\theta_2\right)\right]\left[\cos\left(\theta_1-\theta_2\right) - \cos\theta\right]}} + g(p,\theta)\,.\end{aligned} \tag{3}$$

The integration region in (3) is determined by the conditions

$$|\theta_1 - \theta_2| \leqslant \theta\,, \qquad \theta \leqslant \theta_1 + \theta_2 \leqslant 2\pi - \theta\,. \tag{4}$$

The nonlinear integral term represents the two-particle intermediate states of the incoming particles. The function

$$g(p,\theta) \propto \sum_i \int \mathrm{d}\Phi_i\, M_i M_i^*(\theta) \tag{5}$$

represents the shadowing contribution of the inelastic processes to the imaginary part of the elastic scattering amplitude. Following [7], it is called the overlap function. It defines the overlap within the corresponding phase space $\mathrm{d}\Phi_i$ between the matrix element M_i of the ith inelastic channel and its conjugate counterpart with the collision axis of initial particles turned through the proton scattering angle θ in the elastic process. It is positive at $\theta = 0$ but can change sign at $\theta \neq 0$ due to the relative phases of inelastic matrix elements M_i.

At $t = 0$, relation (3) leads to the optical theorem

$$\operatorname{Im} f(s,0) = \frac{\sigma_{\mathrm{t}}}{4\sqrt{\pi}} \tag{6}$$

and to the general statement that the total cross section is the sum of cross sections of elastic and inelastic processes,

$$\sigma_{\mathrm{t}} = \sigma_{\mathrm{el}} + \sigma_{\mathrm{in}}\,, \tag{7}$$

i.e., that the total probability of all processes is equal to unity.

This allows estimating the real and imaginary parts separately just in the forward direction $t = 0$ after the values of ρ_0 and σ_{t} are measured.

The real and imaginary parts of the amplitude are in general related at any t by the dispersion relations as parts of an analytic function. This approach was used for predictions of the energy behavior of ρ_0 and was only successful at the qualitative level, because its accuracy depends on extrapolations of $\operatorname{Im} f(s,0)$ and, consequently, of σ_{t} to higher energies. A similar treatment at arbitrary values of t requires some additional assumptions, and the conclusions strongly depend on them.

The theoretical approaches differ in ascribing different roles for the relative contributions of the real and imaginary parts at $t \neq 0$. Unfortunately, the available tools are rather modest and cannot exploit the power of QCD at full strength. Elastic scattering implies that the same hadrons are observed in the final state, which means that the partons inside them act collectively, while QCD methods are applicable to incoherent interactions of individual partons at high transferred momenta. Therefore, the phenomenological models and some insights from the unitarity relation are mostly used.

From experiment, we also know the energy behavior of the real and imaginary parts of the amplitude (or their ratio $\rho(s,0) = \rho_0$) in the forward direction $t = 0$. At high energies, this ratio is rather small. For proton–proton scattering, it is negative at lower energies (reaching values about -0.3), becomes equal to zero at energies about 100 GeV, exhibits a positive maximum and decreases to about 0.1 at the LHC energy 7 TeV. Most phenomenological models aim to fit experimental data on the differential cross section and the ratio $\rho(s,0)$ in a wide energy range and to predict them at higher energies. We still cannot claim that the desired aim has been achieved, as can be seen, in particular, in Fig. 1b, where the failure of predictions of five theoretical models at 7 TeV is shown, even though all of them were quite successful at lower energies.

This situation is described in more detail in review paper [6], and we do not repeat it here. Instead, we concentrate on the two important problems described above.

3. Geometry of the interaction region

The structure of protons is one of the main problems in particle physics. It is well known [8] that there is currently a $\approx 7\sigma$ disagreement between the proton charge radius determined from muonic hydrogen and that from electron–proton systems: atomic hydrogen and e$-$p elastic scattering. The partonic structure of protons is successfully studied in deep inelastic electron–proton collisions. The point-like nature is

ascribed to the colliding electron. Therefore, the interaction region is defined by the proton size. Its size and opacity (or darkness) are determined by the Fourier image of the generalized parton distribution functions of protons depending on the total energy and the virtuality of the exchanged photon measured in experiment. Both the size and the opacity evolve with energy, because the parton content of the proton evolves.

In proton–proton, as well as in proton–nucleus and nucleus–nucleus collisions, both objects have some complicated internal structure. The partons of one of them can interact with many partons of the other, distributed somehow within some spatial volume. Moreover, there can be coherent interactions of some groups of partons. It is therefore difficult to disentangle the individual contributions. The correlation femtoscopy, using its correspondence to the Hanbury–Brown and Twiss intensity interferometry, well known in astrophysics, is widely used in studies of the space–time structure in inelastic processes. Correlations between the momenta of newly created particles (mostly pions) reveal the spatial structure of the interaction region. This technique is especially successful in application to nuclei but meets some problems [9] for smaller objects like protons, due to the Heisenberg uncertainty relation. The uncertainty limit is about 1 fm for current high-energy experiments. The coherence of individual sources should be taken into account for such systems.

Here, we show that it is possible to study the spatial structure of the interaction region of colliding protons even at smaller distances using information about their elastic scattering. We discuss the transverse size of this region. We do not consider the longitudinal and temporal sizes, because they are closely related to the model-dependent assumptions on the partonic structure of protons (the relative contributions of partons with definite shares of the longitudinal momentum). In fact, the role of the generalized parton distribution functions integrated over the longitudinal momenta is to be studied. Experimental results on the properties of the diffraction cone, which automatically account for the nonperturbative dynamics of the process and coherence of unknown internal sources, determine the main features of the transverse structure. The parameters obtained from experimental data on elastic processes are directly related to the properties of this region such as its transverse size and opacity (or blackness). Their energy dependence determines its evolution with the collision energy.

To define the geometry of the collision, all characteristics defined in terms of the angle θ and the transferred momentum t must be reexpressed in terms of the transverse distance between the centers of the colliding protons, called the impact parameter b. This can be easily done by the Fourier–Bessel transform of the amplitude f, which retranslates the momentum data to the transverse space features and is written as

$$\mathrm{i}\Gamma(s,b) = \frac{1}{2\sqrt{\pi}}\int_0^\infty \mathrm{d}|t|\, f(s,t)\, J_0\bigl(b\sqrt{|t|}\,\bigr)\,, \tag{8}$$

where J_0 is the Bessel function.

The unitarity condition in the b-representation is given by

$$G(s,b) = 2\,\mathrm{Re}\,\Gamma(s,b) - \bigl|\Gamma(s,b)\bigr|^2\,. \tag{9}$$

The left-hand side (the overlap function in the b-representation) describes the transverse impact-parameter profile of inelastic collisions of protons. It is just the Fourier–Bessel transform of the overlap function g. It satisfies the inequalities $0 \leqslant G(s,b) \leqslant 1$ and determines how absorptive the interaction region is, depending on the impact parameter (with $G = 1$ for full absorption and $G = 0$ for complete transparency). The profile of elastic processes is determined by the subtrahend in Eqn (9). If $G(s,b)$ is integrated over the impact parameter, it leads to the cross section of inelastic processes. The terms in the right-hand side would respectively produce the total cross section and the elastic cross section, as should be the case according to Eqn (7). The overlap function is often shown in relation with the opacity (or the eikonal phase) $\Omega(s,b)$, such that $G(s,b) = 1 - \exp\bigl(-\Omega(s,b)\bigr)$. Thus, full absorption corresponds to $\Omega = \infty$ and complete transparency to $\Omega = 0$.

Even though the impact parameter cannot be measured directly, the geometric picture is instructive and closely related to experimentally found characteristics such as the ratio of the diffraction cone slope to the total cross section, which provides immediate guides to its energy evolution. The impact parameter profiles of elastic and inelastic hadron collisions are derived as Fourier–Bessel transforms of measurable data. They help us visualize the geometric picture of partonic interactions, indicating their spatial extension and the intensity. Our intuitive guesses about the space–time development of these processes can be corrected in this way.

The diffraction cone contributes mostly to the Fourier–Bessel transform of the amplitude. Using the above formulas, we can write the dimensionless quantity Γ as

$$\mathrm{i}\Gamma(s,b) = \frac{\sigma_\mathrm{t}}{8\pi}\int_0^\infty \mathrm{d}|t|\exp\left(-\frac{B|t|}{2}\right)\bigl(\mathrm{i}+\rho(s,t)\bigr)\,J_0\bigl(b\sqrt{|t|}\,\bigr)\,. \tag{10}$$

Here, the diffraction cone approximation (2) is inserted. From this,

$$\mathrm{Re}\,\Gamma(s,b) = \frac{1}{Z}\exp\left(-\frac{b^2}{2B}\right) \tag{11}$$

is calculated, where we introduce the dimensionless ratio of the cone slope (or the elastic cross section) to the total cross section:

$$Z = \frac{4\pi B}{\sigma_\mathrm{t}} \approx \frac{\sigma_\mathrm{t}}{4\sigma_\mathrm{el}}\,. \tag{12}$$

This dependence on the impact parameter was used, in particular, in [10]. Possible small deviations from the exponential behavior (see, e.g., [3, 4]) inside the cone barely change the value of the integral contribution. The differential cross section is quite small outside the diffraction peak and does not influence the impact parameter profile G. Therefore, our first problem turns out to be practically independent of the second problem.

As was mentioned, the ratio $\rho(s,t)$ is very small at $t = 0$, and we first neglect it and obtain

$$G(s,b) = \frac{2}{Z}\exp\left(-\frac{b^2}{2B}\right) - \frac{1}{Z^2}\exp\left(-\frac{b^2}{B}\right). \tag{13}$$

For central collisions with $b = 0$, this gives

$$G(s,b=0) = \frac{2Z-1}{Z^2}\,. \tag{14}$$

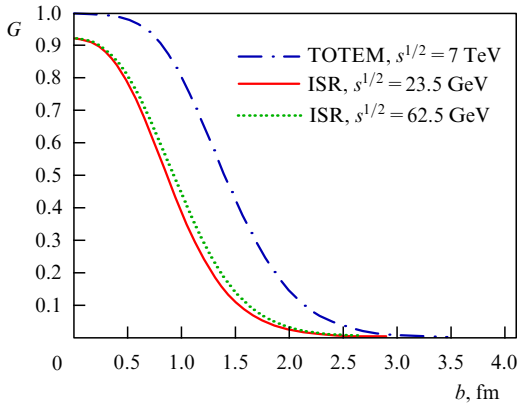

Figure 2. Overlap function $G(s, b)$ at 7 TeV (upper curve) [11] compared to those at ISR energies 23.5 GeV and 62.5 GeV (all of them are computed by using the fit of experimental data according to the phenomenological model in [12]).

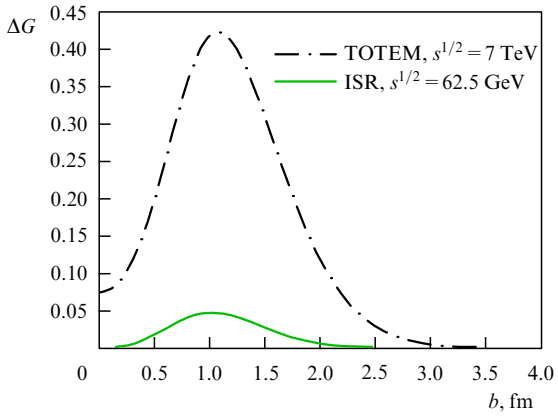

Figure 3. Difference between the overlap functions at different energies [11, 12]. Dashed-dotted curve is for 7 TeV and 23.5 GeV energies, solid curve is for 62.5 GeV and 23.5 GeV. Conclusion: The parton density at the periphery strongly increases!

This formula is very important because it implies that the darkness at the very center is fully determined by the parameter Z, the ratio of experimentally measured characteristics — the width of the diffraction cone B (or $\sigma_{\rm el}$) and the total cross section. Their energy evolution defines the evolution of the absorption value. The interaction region becomes completely absorptive, $G(s, 0) = 1$, in the center only at $Z = 1$, and the absorption diminishes for other values of Z.

In Table 1, we show the energy evolution of Z and $G(s, 0)$ for p–p and p$-\bar{\rm p}$ scattering as calculated from experimental data on the total cross section and the diffraction cone slope at corresponding energies. We note that starting from the ISR energies, the value of Z decreases systematically and at the LHC energies becomes equal to 1 within the accuracy of measurements of B and $\sigma_{\rm t}$.

The impact parameter distribution of $G(s, b)$ in (13) has its maximum at $b_{\rm m}^2 = -2B \ln Z$ with the full absorption $G(b_{\rm m}) = 1$. Its position depends on both B and Z.

We note that for $Z > 1$, we have incomplete absorption $G(s, b) < 1$ at any physical $b \geqslant 0$, with the largest value reached at $b = 0$, because the maximum occurs at nonphysical values $b < 0$. The disk is semitransparent.

At $Z = 1$, the maximum is positioned exactly at $b = 0$, and the absorption is absolutely strong there: $G(s, 0) = 1$. The disk center becomes impenetrable (black).

At $Z < 1$, the maximum shifts to positive physical impact parameters. A dip is formed at the center, which leads to the concave shape of the inelastic interaction region, approaching a toroid shape. It becomes deeper at smaller Z. The limit value $Z = 0.5$, leading to complete transparency at the center $b = 0$, is considered in more detail below.

The maximum absorption in central collisions, $G(s, 0) = 1$, is reached at the critical point $Z = 1$, which is the case at the LHC energy $\sqrt{s} = 7$ TeV, as seen from Table 1. This case is therefore considered first. Moreover, the strongly absorptive core of the interaction region grows in size, as we see from the expansion of Eqn (13) at small impact parameters:

$$G(s, b) = \frac{1}{Z^2}\left[2Z - 1 - \frac{b^2}{B}(Z - 1) - \frac{b^4}{4B^2}(2 - Z)\right]. \quad (15)$$

The second term proportional to b^2 vanishes at $Z = 1$, and $G(b)$ develops a plateau that extends to quite large values of b, about 0.4–0.5 fm. The plateau is very flat because the third term starts to play a role at 7 TeV (where $B \approx 20$ GeV^{-2}) only at even larger values of b. The structure of the interaction region with a central core at energies of 7–8 TeV is also supported (see Fig. 2, where it is compared with corresponding structures at the ISR energies) by direct computation [11] using the experimental data of the TOTEM collaboration [1, 2] about the differential cross section in the region $|t| \leqslant 2.5$ GeV^2.

The results of analytic calculations according to (13) and of the direct computation practically coincide (see Fig. 1 in [13]). It was also shown in [13] that this two-component structure with the central black core and more transparent periphery is well fitted by the expression with an abrupt (Heaviside-like) change of the exponential. However, it is still quite far from the black-disk limit, because the peripheral region at b near 1 fm is very active and shows a strong increase compared to the ISR energies [11]. This is demonstrated in Fig. 3, where the difference $\Delta G(b) = G(s_1, b) - G(s_2, b)$ between the overlap functions at different energies s_1 and s_2 is displayed.

The lower plot in Fig. 3, obtained in [12], demonstrates that even within the quite narrow interval of ISR energies, the role of peripheral interactions with the impact parameters about 1 fm increases in inelastic processes with an energy increase. Even more spectacular is the peripheral increase in passing from ISR to LHC energies, as seen in the upper plot in Fig. 3. Moreover, the darkness of the central core strongly increases in Figs 2 and 3, which becomes especially important, as we discuss in detail in the next section.

Table 1. Energy behavior of Z and $G(s, 0)$.

$\sqrt{s}$, GeV	2.70	4.11	4.74	7.62	13.8	62.5	546	1800	7000
Z	0.64	1.02	1.09	1.34	1.45	1.50	1.20	1.08	1.00
$G(s, 0)$	0.68	1.00	0.993	0.94	0.904	0.89	0.97	0.995	1.00

It is interesting that the positivity of $G(s,b)$, i.e., of $\sigma_{\rm inel}(s,b)$, imposes some limits on the relative role of B and $\sigma_{\rm t}$. Namely, it follows from Eqn (14) that

$$2Z = \frac{8\pi B}{\sigma_{\rm t}} = \frac{\sigma_{\rm t}}{2\sigma_{\rm el}} \geqslant 1\,. \tag{16}$$

This relation implies that the slope B should increase with energy at least as rapidly as the total cross section $\sigma_{\rm t}$.

This inequality is fulfilled at present-day and intermediate energies. If the value of Z decreases at energies above 7 TeV, as could be expected from its tendency shown in Table 1, and approaches $Z = 0.5$, then this inequality can be saturated. We first discuss what happens in the region $0.5 \leqslant Z \leqslant 1$. The values $Z < 0.5$ are addressed at the end of this section.

It is usually stated that the equality $2Z = 8\pi B/\sigma_{\rm t} = \sigma_{\rm t}/(2\sigma_{\rm el}) = 1$ corresponds to the black-disk limit. Certainly, the equality of elastic and inelastic cross sections is fulfilled: $\sigma_{\rm el} = \sigma_{\rm inel} = 0.5\sigma_{\rm t}$. However, in addition to this equality, the scattering on the black disk should result in a special nonexponential shape of the differential cross section like

$$\frac{{\rm d}\sigma}{{\rm d}t} \propto \frac{J_1^2\bigl(R\sqrt{|t|}\bigr)}{|t|}\,, \tag{17}$$

where J_1 is the Bessel function. It has a zero at $|t| \approx 3.67/B$ if the relation $R^2 = 4B$ is used. At the energy of 7 TeV, this zero should be placed at $|t| = 0.3$ GeV^2, which is not confirmed by experiment; neither is the equality of cross sections of elastic and inelastic collisions confirmed experimentally.

In principle, we cannot exclude a possible fast replacement of the regime of the exponential decrease in the diffraction cone (2) by a new one. The appearance of another steeper exponential at the end of the diffraction cone in Fig. 1a at 7 TeV and the noticeable shift of the dip position to smaller transferred momenta at the LHC compared to lower energies could be the first signs of it.

Nevertheless, we continue to study the situation assuming that the exponential regime valid up to the LHC energies persists at higher energies. We see from Eqn (14) that $G(s,b=0) = 0$ at $Z = 0.5$, i.e., the inelastic interaction region is completely transparent in central collisions. Of course, it should not be called a black disk. This paradox is resolved [14] if we write the inelastic profile of the interaction region using Eqn (13). At $Z = 0.5$, it is

$$G(s,b) = 4\left[\exp\left(-\frac{b^2}{2B}\right) - \exp\left(-\frac{b^2}{B}\right)\right]. \tag{18}$$

We see that the black disk must be renamed a black toroid (or a black ring if we consider its two-dimensional projection) with full absorption $G(s,b_{\rm m}) = 1$ at the impact parameter $b_{\rm m} = R\sqrt{0.5\ln 2} \approx 0.59R$, complete transparency at $b = 0$, and a rather large half-width of about $0.7R$. Thus, the evolution to values of Z smaller than 1 at higher energies (this can happen if the tendency of Z to decrease with energy, shown in Table 1, persists) would imply a quite special transition from the critical two-scale regime at the LHC energy to concave toroid-like (or ring-like in two dimensions) configurations of the interaction region if the exponential shape of the diffraction cone described by Eqn (2) persists.

It looks as if the protons penetrate through one another in central collisions, just scattering elastically, while peripheral collisions become responsible for inelastic processes. Elastic and inelastic profiles become equal only at $b = b_{\rm m}$. The elastic one dominates at $b < b_{\rm m}$, while the inelastic one dominates at the periphery, $b > b_{\rm m}$.

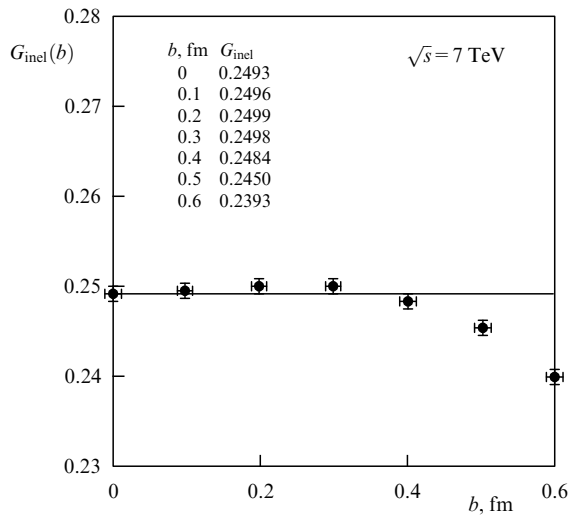

Figure 4. Impact parameter dependence of the function $G_{\rm inel}(b) = 0.25G(b)$ at 7 TeV [15]. It is obtained using the fit of experimental data according to the model in [12].

Is the parton coherence inside each colliding proton responsible for that? Can we observe its effects similarly to the difference between light scattering in water (coherence!) and in air? (Decoherence and fluctuations are responsible for the blue color of the sky!)

Paradoxically enough, this pushes us back to the early suggestions that inelastic processes are more peripheral (recall the one-pion exchange model!) than elastic scattering, which is a shadow of inelastic interactions (more pions exchanged). This tendency is clearly seen already at present-day energies, as demonstrated in Fig. 3. We stress that the total region of proton interactions preserves the Gaussian shape described by the first term in the right-hand side of Eqn (13). The Gaussian shape is also preserved for the elastic profile, but with an exponential that is twice as steep [see Eqns (13) and (18)].

Concerning the longitudinal distances, it is commonly assumed in the parton model that they are much larger than the transverse size, especially for soft partons. Then the region of inelastic interactions would just resemble a toroid, i.e., a tube, at the center of which only elastically scattered protons fly.

The plateau of $G(b)$ at small b was confirmed in [15], as shown in Fig. 4. However, an additional substructure at the level of 10^{-4} at a single point was mentioned there. The function $G_{\rm inel} = 0.25G$ at 7 TeV, plotted there, slightly decreases at $b = 0$ compared to its values at $b = 0.1-0.3$ fm (compare the numerical values shown in Fig. 4). This could be an indication that Z becomes somewhat less than 1 already at 7 TeV and the transition to the concave shape starts at this energy. At the same time, no decrease is seen in Fig. 2. This disagreement is especially surprising because the same model [12] was used in papers [11, 15] to fit experimental results at 7 TeV. However, we see that the excess at impact parameters 0.1–0.3 fm compared to the center, pointed out in [15], reveals itself in the fourth digits only, while the error bars of the slope B and the total cross section $\sigma_{\rm t}$ are larger by an order of magnitude. This excess is so small that it can be explained either by insufficient precision in determining the values of B and $\sigma_{\rm t}$ (and, consequently, of Z) and by inaccuracy in

accounting for different scales or by different procedures adopted in [11, 15] for extrapolations to the ranges of transferred momenta where there are no experimental data yet.

Therefore, it seems too early to make any statements (even preliminary ones). However, a comparison of the results in [11] and [15] shows that we are in the critical regime of elastic scattering with $Z \approx 1$ at 7 TeV, as was pointed out in [14]. We stress that, with good precision of the experimental data, the proposed approach allows analyzing the fine structure of the core of the interaction region at very small scales, as opposed to the less precise correlation methods. Therefore, we should pay special attention to the evolution of the parameter Z at the higher energy 13 TeV, which will become available soon. Especially precise measurements of the diffraction cone slope B and the total cross section σ_t would be very desirable.

Another consequence of Eqn (14) follows from a study of the energy evolution of $G(s,0)$, shown in Table 1. In connection with the torus-like concave structure, it is interesting to note the value $Z = 0.64$ or $G(s,0) = 0.68$ at $\sqrt{s} = 2.70$ GeV and the maximum $G = 1$ at $b_m^2 = 4B\ln 2$. However, at this rather low energy, the whole analysis should be redone with the diffraction cone behavior, the total cross section, and the value of the ratio ρ taken into account. We also note that in the energy interval $4 < \sqrt{s} < 8$ GeV, the values of Z are slightly larger than 1, such that the values of $G(s,0)$ are smaller than but very close to 1. These facts require further studies in the energy interval $2.7 < \sqrt{s} < 8$ GeV, especially in view of the proposed experiments in Protvino. The dark core must be smaller at lower energies than at the LHC energy because of smaller values of B. Moreover, the contribution due to the real part of the amplitude is larger at these energies, and the larger $|t|$ beyond the diffraction cone can be important.

The dependence of Z on energy shown in Table 1 looks as if the interaction region at low energies becomes black at the center $b = 0$, but at higher energies, up to the ISR ones, it loses this property, trying to restore it at the LHC energy.

In principle, the positivity of the inelastic cross section

$$\sigma_{\text{inel}} = \frac{\pi B}{Z^2}(4Z - 1) \geqslant 0 \tag{19}$$

allows values of Z as small as 0.25, which corresponds to $\sigma_{\text{el}} = \sigma_t$ and $\sigma_{\text{inel}} = 0$. The values $Z < 0.5$ lead to negative values of $\sigma_{\text{inel}}(s,b)$, i.e., to negative Fourier–Bessel transforms of $g(p,\theta)$ in Eqn (5). They are not forbidden if the relative phases of matrix elements of inelastic processes M_i in Eqn (5) interfere in such a way. Unfortunately, we have no knowledge about them. This possibility was treated as another branch of the solution of the unitarity condition and named anti-shadowing or refractive scattering in [16] and resonant disk modes in [17]. However, the value of Z is close to 1 even at the LHC energies, and this regime requiring $Z < 0.5$ is certainly shifted to extremely high energies if it can be observed at all. The approach to the asymptotic regime is typically assumed to follow the logarithmic dependences of cross sections $\sigma_t \propto \sigma_{\text{el}} \propto \ln^2 s$ and $\sigma_{\text{inel}} \propto \ln s$. The depletion of $G(s,0)$ in [15] was ascribed to this regime by mistake, because the values of Z at 7 TeV are near 1 but not as small as 0.5.

4. New tendencies of inelastic collisions

The maximum absorption in central collisions at LHC energies must reveal itself in some special features of inelastic collisions in such a critical regime with $Z \approx 1$. The diffraction cone contributes mostly to $G(s,b)$. The large-$|t|$ elastic scattering cannot serve as an effective trigger of the black core. One of the typical features of high-energy inelastic processes is the production of high-energy jets, i.e., collimated groups of particles. Inelastic exclusive processes can be more effectively used for the analysis of the central black core. Such triggers that enhance its contribution are needed. Following the suggestions in [10, 18], it has become possible [13] to study the details of the central core using the experimental data of the CMS (Compact Muon Solenoid) collaboration at 7 TeV on inelastic collisions with high multiplicity triggered by hadron jet production [19], as well as some other related data. Triggers (charged particles or jets) with large transverse momenta are produced in central collisions. Therefore, the black plateau in the central part of the interaction region with $b < 0.4-0.5$ fm should result in the corresponding plateau of the charged-particle density in the transverse region $60^\circ < |\Delta\phi| < 120^\circ$, defined as

$$\mu_{\text{tr}} = \frac{N_{\text{ch}}^{\text{tr}}}{\Delta\eta\Delta(\Delta\phi)}\,, \tag{20}$$

where $N_{\text{ch}}^{\text{tr}}$ is the charged particle multiplicity in the transverse region, $\Delta\eta$ is the pseudorapidity range studied, and $\Delta(\Delta\phi)$ is the azimuthal width of the transverse region. This is indeed the case, as shown in Fig. 5.

We explain. Starting from large transverse momenta of triggers on the right-hand side of Fig. 5 and going to the left, we first sort of probe the central region from $b = 0$ to the end of the plateau. Then the density of accompanying particles in the transverse region should not change until we approach the end of it. Only then should the decrease in the distribution of the accompanying particles start. The difference in positions of such a decrease in the two plots is defined by the difference in the choice of the leading trigger used by the two collaborations, CMS and ALICE (A Large Ion Collider Experiment). The flat dependence of μ_{tr} on p_t shows that activity in the transverse region is independent of the hard process scale if the scale is hard enough for all proton–proton interactions to be central.

Many other characteristics of such inelastic processes considered in [13] support this conclusion. The use of very

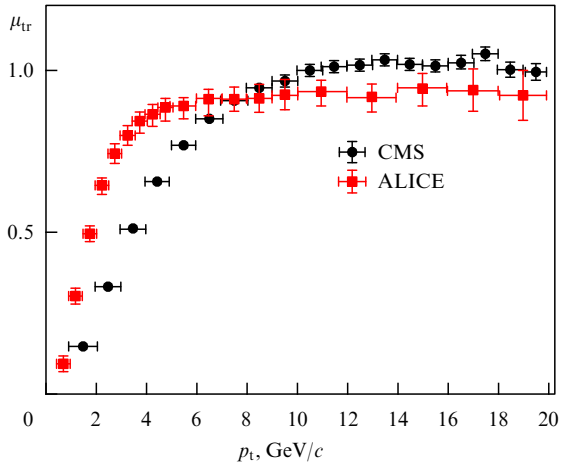

Figure 5. Charged-particle density in the transverse region as a function of p_t of the leading object [13] (CMS — charged-particle jet, ALICE — charged particle). CMS analyzes particles with $p_t > 0.5$ GeV/c and $|\eta| < 2.4$, ALICE analyzes those with $p_t > 0.5$ GeV/c and $|\eta| < 0.8$.

high-multiplicity events in combination with jet properties is crucial. In particular, the most important observation is that a significant reduction in the jet rate at very high multiplicities compared to MC predictions requires new inputs in the models. Separating the core contribution with the help of these triggers, we arrive at the important conclusion that the simple increase in the geometrical overlap area of the colliding protons does not account for the properties of jet production at very high multiplicities. It looks as if the parton (gluon) density must strongly increase in central collisions, and rare configurations (fluctuations) of the partonic structure of protons are involved. So far, paper [13] remains the only attempt to explain the distinctive features of jets and underlying event properties at LHC energies. The correlation studies of jets (see, e.g., [20]) can be used for further femtoscopy of the fine-structured system. Without a doubt, some further proposals to study the critical regime at 7–8 TeV will be put forward.

At the same time, implications of the energy evolution of Z (if observed!) for inelastic processes are of great interest. The shares of elastic and inelastic cross sections will start approaching one another if the values of Z decrease below 1 with an increase in energy. The mean multiplicity will probably decrease because of the more peripheral origin of newly created particles. The decreasing role of central interactions can lead to some changes in the shape of the multiplicity distributions (lower tails?) and diminished share of jets, which will acquire new features. Jets will become produced at the periphery, in distinction to the situation described above. That would imply that they will have to penetrate larger distances in the transverse direction than in the forward directions. This would give rise to their stronger depletion in the transverse plane and therefore to the azimuthal asymmetries, which were sought in [20]. Of course, other criteria of the transition to the concave shape of the interaction region of inelastic processes will be found.

We will hardly be able to reach a regime with extremely small values $Z < 0.5$ when inelastic processes would play a negligibly small role compared to elastic ones.

5. Elastic scattering outside the diffraction cone

This problem has attracted special attention since the 1960s, when experimental data on the differential cross section at high energies and rather large transferred momenta appeared for the first time. It was observed that the exponential t-regime in the diffraction cone is replaced by the exponential $\sqrt{t}$-regime at larger angles. The latter region of angles was called the Orear region, after its investigator.

The unitarity condition happened to be very successful in that region of angles as well. Theoretically, it can be approached considering the unitarity condition (3) directly in s, t variables without using the Fourier–Bessel transform, as was done at small angles. It was shown a long time ago [5, 21] that the imaginary part of the amplitude f outside the diffraction cone can be derived from the general unitarity condition (3), which reduces there to the inhomogeneous linear integral equation

$$\operatorname{Im} f(p,\theta) = \frac{p\sigma_{\mathrm{t}}}{4\pi\sqrt{2\pi B}} \int_{-\infty}^{+\infty} \mathrm{d}\theta_1 \, \exp\left(-\frac{Bp^2(\theta-\theta_1)^2}{2}\right) \times r_\rho \operatorname{Im} f(p,\theta_1) + g(p,\theta)\,, \tag{21}$$

where $r_\rho = 1 + \rho(s,0)\,\rho(s,\theta_1)$. This reduction becomes possible because the contribution from the asymmetric configuration of scattering angles in the first term in Eqn (3) dominates due to the steep Gaussian fall-off inside the diffraction cone. Because of the sharp fall-off of the amplitude with the angle, the leading contribution to the integral arises from a narrow region around the line $\theta_1 + \theta_2 \approx \theta$. Therefore, the values of one of the amplitudes should be taken at small angles within the cone as Gaussian, while the other amplitude is kept at angles outside the cone.

Equation (21) can be solved analytically (for more details, see [5, 21]) under two assumptions: that the role of the overlap function $g(p,\theta)$ is negligible outside the diffraction cone and that the function r_ρ can be approximated by a constant, i.e., $\rho(\theta_1) = \rho_1 = \text{const}$.

We assume that the overlap function is negligible at these transferred momenta.[1] Then the eigensolution of the homogeneous linear integral equation is

$$\operatorname{Im} f(p,\theta) = C_0 \exp\left(-\sqrt{2B\ln\frac{Z}{r_\rho}}\,p\theta\right) + \sum_{n=1}^{\infty} C_n \exp\left[-(\operatorname{Re} b_n)p\theta\right] \cos\left(|\operatorname{Im} b_n|\,p\theta - \phi_n\right), \tag{22}$$

with

$$b_n \approx \sqrt{2\pi B|n|}\,(1 + \mathrm{i}\,\operatorname{sign} n)\,, \quad n = \pm1, \pm2, \ldots\,. \tag{23}$$

This expression contains a term exponentially decreasing with θ (or $\sqrt{|t|}$) (the Orear regime!) with the oscillations imposed on it more strongly damped by their own exponential factors b_n compared with the first term. The critical role in the exponent of the first leading term, which determines the rate of decrease in the differential cross section, is again played by the parameter Z widely used above Eqn (12). The oscillating terms become pronounced only at smaller angles and reveal themselves as a dip in the vicinity of the diffraction cone. The elastic scattering differential cross section outside the diffraction cone (in the Orear regime region) is

$$\frac{\mathrm{d}\sigma}{p_1\,\mathrm{d}t} = \left[\exp\left(-\sqrt{2B|t|\ln\frac{Z}{r_\rho}}\right) + p_2 \exp\left(-\sqrt{2\pi B|t|}\right)\cos\left(\sqrt{2\pi B|t|} - \phi\right)\right]^2, \tag{24}$$

with the parameters p_1 and p_2 closely related to C_0 and C_1. Just this formula was used in Refs [11, 24] for fits of experimental data on differential cross sections in a wide energy range. The ratio ρ was approximated by its average values in and outside the diffraction cone, such that $r_\rho = 1 + \rho_0\rho_1$, where ρ_1 is treated as the average value of ρ in the Orear region.

The fits at comparatively low energies [24] are consistent with $r_\rho \approx 1$, i.e., with small values of ρ_1 close to zero. When

[1] The assumption on the smallness of the overlap function outside the diffraction cone is appealing intuitively: particles newly created in high-energy inelastic processes move mainly inside narrow angular cones along the directions of the primary hadrons. Therefore, the geometric overlap of two narrow cones whose axes are rotated through a comparatively large angle θ, is negligibly small. Moreover, this assumption has been confirmed [22, 23] by direct computation of the overlap function from experimental data in a wide energy interval up to the LHC energies.

$Z = 1$, as happens at 7 TeV (see Table 1 above), the exponent of the leading first term is very sensitive to the value of ρ_1 outside the diffraction cone. For the first time, that allowed estimating the value of ρ in the Orear region at 7 TeV [23]. The great surprise of the fit of TOTEM data was the necessity of using the large (in modulus) negative value $\rho_1 \approx -2.1$ if $\rho_0 = 0.14$ (as it was at ISR energies). Otherwise, the slope of the first term in Eqn (22) in the Orear region would be predicted to be equal to zero (constancy!) if $Z = 1$ and $r_\rho = 1$. It becomes larger in modulus, $\rho_1 \approx -3$, if the TOTEM value $\rho_0 = 0.1$ obtained at 7 TeV is used. Moreover, these values of ρ_1 can be regarded as upper bounds, because the effective value of ρ_0 inside the diffraction cone can be even smaller in view of its widely discussed zero there. No models have yet explained this finding. Further progress in solving the unitarity equation with the proper dependence of ρ inside and outside the diffraction cone is needed.

The slope of the differential cross section in the Orear region becomes a very sensitive indicator of the mutual behavior of Z and ρ_1. A possible decrease in the value of Z with increasing energy and the transition to the torus regime discussed above would require a further evolution of the ratio ρ to negative values increasing in modulus.

The predictive power of solution (22) lies in its exponential behavior in $\sqrt{|t|}$ with a quite definite analytically calculable exponent and oscillations imposed on it. Unfortunately, we cannot definitely state where its bounds on the t axis are, and we have to rely on the accuracy of fits within some range of t. Nevertheless, as was mentioned above, some important estimates of the value of ρ in the Orear region have been made. Another shortcoming of solution (22) is its ignorance of the energy dependence. Therefore, no predictions are made concerning higher energies. Not only are the normalization coefficients C_0 and C_n unknown, but also the exponent of the leading term suffers from the unpredictable energy behavior of B, σ_t, and r_ρ. Only with results on B and σ_t obtained from experiments at higher energies is it possible to estimate the mean value of ρ in the Orear region.

In parallel, there is a variety of phenomenological models with numerous adjustable parameters, proposed in attempts to describe experimental data. The theoretical arguments in favor of them and their main features are reviewed in some detail in [6]. Most of them describe the behavior of the differential cross section in the diffraction cone quite well (albeit with some precaution). Therefore, if applied to the problem, they would reproduce the main features of the shape of the interaction region discussed in the preceding section. The imaginary part of the amplitude dominates there. At the same time, the models failed in their predictions at 7 TeV in the Orear region, as shown in Fig. 1b. The main problem lies in their inability to predict the energy dependence of adjustable parameters. Only some qualitative guesses can be used.

Certainly, it is much easier to use such guesses and to fit these parameters with the newly available data. This was successfully done a posteriori, for example, in [11, 15, 25]. The first two of these papers used the model in [12] proposed long ago, while a completely new form of the amplitude was analyzed in [25].

Independently of the success or failure of these models in describing the Orear region, all of them have a common heuristic feature. To explain prominent characteristics of the differential cross section such as the dip (see Fig. 1b), they have to assume that it originates at the transferred momentum t where the imaginary part of the amplitude (dominating until then within the diffraction cone!) vanishes. The models differ only in the number of zeros in the real and imaginary parts and in their positions, except the definitely fixed t value at the dip.

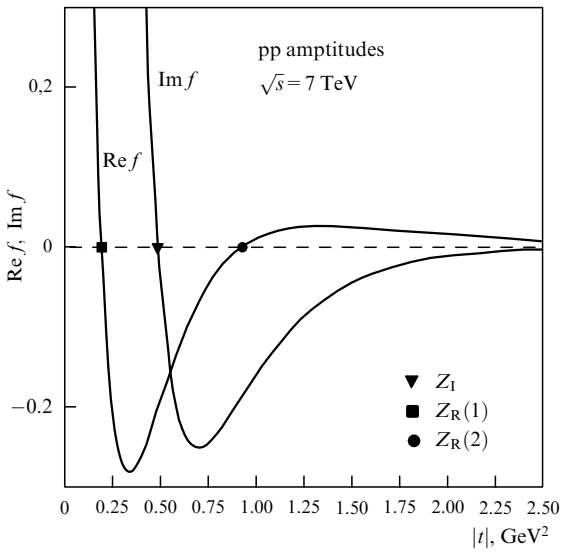

Figure 6. Real (Re f) and imaginary (Im f) parts of the proton–proton amplitude at 7 TeV according to a particular phenomenological model [25].

As an example, in Fig. 6, we show the corresponding plots obtained for the model in [25]. The only zero of the imaginary part at the dip position is marked as Z_I. The real part has two zeros. One of them, $Z_R(1)$, lies within the diffraction cone. This zero is typical for many models and was somehow envisaged in [26, 27], albeit without definite predictions about its position. Its appearance leads to the necessity to diminish the theoretical estimates of the average value of ρ inside the cone, which enters solution (22) as ρ_0 but should be treated, strictly speaking, as the average value of ρ inside the cone. That, in turn, would lead to larger values (in modulus) of ρ_1, as discussed above. The peculiar feature of the model in [25] is that the real part crosses the abscissa axis and has a second zero $Z_R(2)$. Therefore, the ratio ρ becomes negative in the Orear region, although not large enough (in modulus) to correspond to estimates obtained in the unitarity approach. Anyway, there is some correspondence between them at the qualitative level. Other models usually have single zeros of the real and imaginary parts and cannot produce negative values of ρ in the Orear region. Probably, this is the origin of their failure to predict the LHC results.

It is worth stressing here that no zeros of the imaginary part are predicted in the unitarity approach. The dip is explained in [23] as the contribution of the oscillatory terms in (22), whose role increases at smaller transferred momenta. At the same time, we should critically remark that fits of the differential cross section in the Orear region with the help of only the imaginary part of the amplitude become self-contradictory after the conclusion about the large value of ρ_1 there is obtained. No agreement between these two approaches has been reached yet. In general, we can state that the t dependence of the real and imaginary parts has not yet been understood theoretically.

6. Conclusions

The use of the indubitable general principle — the unitarity condition — in combination with experimental results on elastic scattering in the diffraction cone allows revealing the spatial image of the interaction region of protons and its evolution with energy, as well as for the first time estimating the average value of the real part of the elastic scattering amplitude beyond the diffraction cone.

The behavior of the real and imaginary parts of the elastic scattering amplitude as functions of the energy s and the transferred momentum t completely defines the properties of this process and, in some way, influences the properties of inelastic processes through the unitarity requirement. Our knowledge of this behavior is still quite limited. QCD methods do not work. The general QCD statements and phenomenological models are usually considered.

It is shown that the geometrical spatial shape of the interaction region of protons is mainly determined by their elastic scattering at small angles. The absorption in the interaction region center is determined by a single energy-dependent parameter Z. The region of full absorption extends to quite large impact parameters, 0.5 fm if Z tends to 1. This happens at the LHC energy $\sqrt{s} = 7$ TeV, where the critical two-scale structure (the black central core and the more transparent peripheral region) of the interaction region of protons becomes well pronounced. The sharp separation of these two regions leads to special consequences for both elastic and inelastic processes. The behavior of the parameter Z at higher energies is especially important for the evolution of the geometry of the interaction region. The assumption about its further decrease at higher energies results in a drastic change in the geometry predicting the tendency for evolution to the completely unexpected toroid (tube)-like (or ring-like in two dimensions) configuration, where the core becomes absolutely penetrable and the complete absorption region is shifted to some finite impact parameter.

The value $Z = 1$ attained at the LHC energies is also crucial for the behavior of the elastic scattering differential cross section outside the diffraction cone. In this case, its slope there becomes fully defined by the ratio of the real part of the amplitude to its imaginary part, which is still unknown at the LHC energies in this range of the transferred momenta. No way to its direct measurement is currently foreseen. Therefore, it is very important that the analysis of experimental data at 7 TeV concerning the slope of the differential cross section inside the Orear region with the help of the unitarity condition provide an estimate of its average value and reveal that this ratio is negative and surprisingly large in modulus. The predictions of phenomenological models are contradictory in this region of transferred momenta. In general, these models should be checked for their self-consistency by calculation of the overlap functions $g(p, \theta)$ for each of them. This is possible because the integral in unitarity relation (3) can be computed with both real and imaginary parts of the amplitude for a particular known model. The measurement of the rate of decrease in the differential cross section in the Orear region becomes very important at higher energies, because it happens to be very sensitive to the mutual behavior of Z and ρ_1 with an increase in energy.

Thus, the unitarity condition provides many inspiring guides about hadron interactions, which should be taken into account by other approaches.

We thank the RFBR grants 12-02-91504-CERN-a, 14-02-00099, and the RAS–CERN program for support.

References

1. Antchev G et al. (TOTEM Collab.) *Europhys. Lett.* **95** 41001 (2011)
2. Antchev G et al. (TOTEM Collab.) *Europhys. Lett.* **96** 21002 (2011)
3. Antipov Yu M et al. *Czech. J. Phys. B* **26** 382 (1976)
4. Zotov N P, Rusakov S V, Tsarev V A *Sov. J. Part. Nucl.* **11** 462 (1980); *Fiz. Elem. Chastits At. Yadra* **11** 1160 (1980)
5. Andreev I V, Dremin I M *JETP Lett.* **6** 262 (1967); *Pis'ma Zh. Eksp. Teor. Fiz.* **6** 810 (1967)
6. Dremin I M *Phys. Usp.* **56** 3 (2013); *Usp. Fiz. Nauk* **183** 3 (2013)
7. Van Hove L *Nuovo Cimento* **28** 798 (1963)
8. Kraus E et al. *Phys. Rev. C* **90** 045206 (2014); arXiv:1405.4735
9. Sinyukov Yu M, Shapoval V M *Phys. Rev. D* **87** 094024 (2013)
10. Frankfurt L, Strikman M, Weiss C *Phys. Rev. D* **83** 054012 (2011)
11. Dremin I M, Nechitailo V A *Nucl. Phys. A* **916** 241 (2013)
12. Amaldi U, Schubert K R *Nucl. Phys. B* **166** 301 (1980)
13. Azarkin M Yu, Dremin I M, Strikman M *Phys. Lett. B* **735** 244 (2014)
14. Dremin I M *JETP Lett.* **99** 243 (2014); *Pis'ma Zh. Eksp. Teor. Fiz.* **99** 283 (2014)
15. Alkin A et al. *Phys. Rev. D* **89** 091501(R) (2014)
16. Troshin S M, Tyurin N E *Phys. Lett. B* **316** 175 (1993)
17. Anisovich V V, Nikonov V A, Nyiri J *Phys. Rev. D* **90** 074005 (2014); arXiv:1408.0692
18. Frankfurt L, Strikman M, Weiss C *Phys. Rev. D* **69** 114010 (2004)
19. Chatrchyan S et al. (CMS Collab.) *Eur. Phys. J. C* **73** 2674 (2013)
20. CMS Collab., PAS FSQ-13-005 (2013)
21. Andreev I V, Dremin I M *Sov. J. Nucl. Phys.* **8** 473 (1968); *Yad. Fiz.* **8** 814 (1968)
22. Andreev I V, Dremin I M, Steinberg D N *Sov. J. Nucl. Phys.* **11** 261 (1970); *Yad. Fiz.* **11** 468 (1970)
23. Dremin I M, Nechitailo V A *Phys. Rev. D* **85** 074009 (2012)
24. Andreev I V, Dremin I M, Gramenitskii I M *Nucl. Phys. B* **10** 137 (1969)
25. Kohara A K, Ferreira E, Kodama T *Eur. Phys. J. C* **73** 2326 (2013); arXiv:1408.1599
26. Martin A *Lett. Nuovo Cimento* **7** 811 (1973)
27. Martin A *Phys. Lett. B* **404** 137 (1997)